Journal Name

ARTICLE

NEWTONIAN TO NON-NEWTONIAN FLUID TRANSITION OF A MODEL TRANSIENT NETWORK

Received 00th January 20xx,
Accepted 00th January 20xx

DOI: 10.1039/x0xx00000x

www.rsc.org/

Giovanni Nava[a], Tie Yang[b], Valerio Vitali[c], Paolo Minzioni[c], Ilaria Cristiani[c], Francesca Bragheri[d], Roberto Osellame[d], Lucas Bethge[e], Sven Klussmann[e], Elvezia Maria Paraboschi[f], Rosanna Asselta[f,g], and Tommaso Bellini[a,*]

The viscosity of gel-forming fluids is notoriously complex and its study can benefit from new model systems that enable a detailed control of the network features. Here we use a novel and simple microfluidic-based active microrheology approach to study the transition from Newtonian to non-Newtonian behavior in a DNA hydrogel whose structure, connectivity, density of bonds, bond energy and kinetics are strongly temperature dependent and well known. In a temperature range of 15 °C, the system reversibly and continuously transforms from a Newtonian dispersion of low-valence nanocolloids into a strongly shear-thinning fluid, passing through a set of intermediate states where it behaves as a power-law fluid. We demonstrate that the knowledge of network topology and bond free energy enables to quantitatively predict the observed behavior using established rheology models.

1. Introduction

Non-Newtonian viscosity is a general feature of multiscale, multicomponent or structured fluids ranging from polymer melts to colloidal dispersions. Among them, physical gels, such as solutions of associating polymers, reversible hydrogels, and in general supramolecular transient networks, are known to display shear-thinning viscosity for large enough shear rates[1–6]. This class of materials also includes biomolecular networks that provide key structural properties to cells and tissues,[7,8]. While it is clear that the shear-thinning of transient networks reflects their internal connectivity and the strength of the bonds, its quantitative Interpretation is a challenge because of the complexity of the systems where it is observed, whose microscopic topology, interaction energies and bonds lifetimes are generally known only in terms of statistical distributions[9–11]. In this context, the introduction of a model system having a well-defined topology and mesh size together with a fully known and controllable density of bonds and bond strength, can offer an unprecedented occasion of clarifying the microscopic mechanisms underlying the emergence of non-Newtonian viscosity.

Here we describe the transition from Newtonian to non-Newtonian behavior of a dispersion of DNA nanoparticles that are independent at high temperature, while they bind into a transient network upon cooling. The nanoparticles are shaped as three-arms nano-stars (NS in the following, Fig. 1a), each arm terminating with a 6-base-long overhang which provides a sticky spot for mutual binding [12]. The network connectivity of this system is thus controlled by the strong temperature (T) dependence of the pairing of the overhangs, which is reliably predictable on the basis of the well-known thermodynamics of DNA hybridization [13]. In a temperature range of 15 °C, the system progressively and reversibly transforms from a solution of single NS or dispersion of clusters (Fig. 1b), to a percolating transient network (Fig. 1c)[12], enabling to explore four order of magnitudes of the Deborah number. The basic idea behind this study is that the emergence of non-Newtonian viscosity is here achieved by the activation of a single class of simple molecular binding events over a temperature range that is so narrow that other equilibrium and dynamic variables are effectively held fixed. We take advantage of the full control of the network structure parameters – including coordination number (f = 3), bond lifetime (τ_B) and binding free energy (ΔG) – to quantitatively understand the transition from linear to shear-thinning viscosity in terms of the stabilization of the tridimensional DNA network. Specifically, we show here that: i) the NS solution displays a gradual and reversible transformation between Newtonian and strongly shear-thinning in a T interval of less of 15 °C; ii) the knowledge of f, τ_B, ΔG, combined either with heuristic arguments or with a rigorous model for the rheology of soft glassy materials [2] enables predicting both the value and the range of T where the transition to shear-thinning

[a] BIOMETRA Department, Università degli Studi di Milano, 20129 Milano, Italy.
[b] School of Physical Science and Technology, Southwest University, Chongqing 400715, China
[c] Department of Information and Industrial Engineering, Università di Pavia, 27100 Pavia, Italy.
[d] Istituto di Fotonica e Nanotecnologie (IFN), Consiglio Nazionale delle Ricerche (CNR), 20133 Milano, Italy
[e] NOXXON Pharma AG, 10589 Berlin, Germany
[f] Department of Biomedical Sciences, Humanitas University, 20089 Pieve Emanuele (MI), Italy
[g] Humanitas Clinical and Research Center, 20089 Rozzano (MI), Italy
† Electronic Supplementary Information (ESI) available: [See DOI: 10.1039/x0xx00000x]

behavior occurs; iii) the behavior at low T can be also quantitatively understood from the topology of the network and ΔG either through a simple geometrical approach or by using the classic Lake-Thomas model[14–16].

2. Materials and Methods

The DNA NS dispersion are prepared by annealing equimolar mixtures of three 48-base-long oligomers. The three sequences self-assemble into three-arms nanoparticles. Each arm is formed by 20 base pairs long duplexes that terminate with 6-base-long overhangs [See ESI]. NS are stable and independent for 40 °C < T < 60 °C, while at lower T the overhangs of distinct NS hybridize so that the NS behave as attractively interacting nanoparticles with valence equal to three [12]. The phase diagram of this system includes a consolution curve separating a vapor-like and a liquid-like phases that terminates in a critical point at T ≈ 11 °C [12]. The coexistence region is limited at DNA concentrations c < 9 mg/ml. At larger concentrations, such as c = 10 mg/ml explored in this study, corresponding to a number density of NS $n_{NS} = 1.34 \cdot 10^{23}$, the NS dispersion transforms, continuously and reversibly, from a liquid of independent particles (at high T), into an arrested gel (at low T) without incurring in phase separations [17]. Such T-controlled gelation is an example of equilibrium gelation, by which the formation of the network is obtained by passing through a set of equilibrium states with no discontinuity [17].

To investigate the viscous behavior of this system across its liquid-gel transition, we used a recently developed microrheological technique based on a microfluidic chip in which a microbead (PMMA, radius R = 5 μm) is trapped at half height of a channel (having square section, 150μm size) and put in motion across the channel by optical forces [20] (Fig. 2a-d). In our design, two counterpropagating beams are carried into the microchannel by two facing waveguides, realized by femto-second laser inscription, that terminate perpendicularly to the channel at half its height [21]. The bead is then held at half channel height by the transversal gradient forces of the two beams. When the intensity of the two beams is unbalanced, the bead also experiences a net scattering force pushing it in the propagating direction of the stronger beam [18,19].

In such stress-controlled microrheological technique, the force on a microbead is easily set and maintained over large bead displacements. This technology is particularly suitable to determine the force-speed ratio and thus to accurately detect the appearance of non-Newtonian behavior.

The laser beams used to apply the optical forces on the PMMA beads, were provided by a CW 10W Yb-doped fiber laser ($\lambda = 1070\ nm$), splitted, coupled to the two counterpropagating waveguides and modulated as explained in Ref. 20. The temperature T of the chip was controlled during all the experiments by a Peltier cell, allowing stability within 0.2 °C and all measurements were performed after 30 min equilibration at each working T. The motion of the bead inside the channel was recorded by a camera (Thorlabs DCC1645C, 20-200 fps) mounted on an inverted microscope, and tracked by a Labview program that also controlled the beam stoppers used to modulate the force on the bead.

The longitudinal force exerted by each beam depends on the x coordinate: $F(x, P_L) = AP_L g(x)$, where P_L is the light power and A is a constant. The profile $g(x)$ was obtained using paraxial optics[22] (Fig. 2e). The product AP_L was determined by calibrating the setup with fluids of known viscosities ranging from 0.001 to $1 Pa\ s$ [20] [see ESI]. We found an excellent repeatability of such calibration procedure, thanks to the monolithic alignment between the optical components and to the laser stability.

Experiments were performed by filling the channel with 1 μL of NS dispersed in 20 mM NaCl aqueous solution at a DNA concentration c = 10 mg/ml, corresponding to a NS molarity $n_{NS} \approx 222\ \mu M$, in which a small number of PMMA microbeads are dispersed.

The experiments are then carried on as in the following. First, one microbead is trapped and positioned close to one side of the microchannel (avoiding contact with the glass wall) by unbalancing the power of the two beams (Fig. 2c). Then, by shutting off the beam emitted from the waveguide farthest to the bead, the bead is pushed across the channel, a procedure that we named "optical shooting" (Fig. 2d). Examples of time-lapse sequence of the bead motion and its position vs. time x(t), are shown in Figs. 2f and 2g. A sufficiently long time is left between two consecutive optical shootings to let the system equilibrate. Thus, in all experiments, the bead always moves within an unperturbed NS dispersion

3. Results and Discussion

Optical shooting experiments were performed at various T in the range (20 - 40 °C) and at various P_L (corresponding to forces in the interval 1-100 pN). Examples of the measured x(t) are shown in Fig. 3a (symbols), each set corresponding to a single optical shooting. Since the inertia of the bead can be neglected, the apparent viscosity η_A of the fluid is determined from x(t) and F(x) via the Stokes law $\eta_A = F(x)/(6\pi R v(x))$ where R is the radius of the bead, and v(x) was computed from x(t). η_A determined at various T is plotted in Fig. 3b as a function of the bead velocity. In some cases – at the largest T – two distinct data sets with same T and different P_L are reported so to explore a wide force range.

As expected, we find the viscosity of the DNA NS solution at the largest T (red dots in Fig. 3b) to be Newtonian, with η_A being independent from v. As T decreases from 40 to 20 °C, two phenomena occur. First, η_A markedly grows, its value at the lowest bead speed increasing of almost 3 orders of magnitude. Second, the system becomes non-Newtonian, η_A progressively acquiring a shear-thinning character. In the explored range of speeds, the apparent viscosity displays a power-law behavior $\eta_A \propto v^{n-1}$, and thus $F \propto v^n$, as evident from the linear behavior of the data in the log-log plot (Figs. 3b and 3c) [23]. The exponent n ranges from 1 (Newtonian limit, largest T) to a value close to 0, as can be appreciated by comparing the data at the lowest T with the -1 slope dashed line. The T dependence of n is shown in Fig. 3f (colored dots, right-hand axis). The rheological

behavior at the lowest T corresponds to the strongest form of shear-thinning viscosity, in which friction becomes independent from speed, as apparent in Fig. 3c, which displays F(v) for the same data as in Fig. 3b.

While in shear cells the shear rate $\dot{\gamma}$ is uniquely set, in bead based experiments a distribution of shear rates is simultaneously probed, as given by the velocity profile of the fluid v(**r**, θ) around the bead, where r is the distance from the bead center (*r*>*R*) and θ the angle with respect of the velocity direction. In Newtonian fluids $v(\mathbf{r}) \propto 1/r$ is the dominant term far from the bead[24] which accounts for the Stokes law. In non-Newtonian shear-thinning power-law fluids in which the viscous friction is $F_{PL} \propto \dot{\gamma}^m$ [23], the velocity profile around a moving bead is modified to $v(\mathbf{r}) \propto 1/r^\alpha$ with $\alpha \approx (2\text{-}m)/m > 1$ and the friction force on the bead becomes $F \propto v^m$ [25]. Thus, despite the intrinsic inhomogeneity of the shear rate induced by the bead motion, our result indicates that, in the explored range, the NS solution is a power law fluid whose exponent equals the one controlling the force on the bead, i.e. m = n.

Power-law fluids are a phenomenological description of the non-Newtonian shear thinning behavior of a fluid, typically verified in limited parameter ranges. When shear rates are small enough, all fluids become Newtonian. In this limit, the equilibration time of the fluid τ, set in our system by the bond lifetime τ_B, is faster than the characteristic time of externally imposed deformations. Non-Newtonian shear thinning behavior can develop when the dimensionless product $\dot{\gamma}\tau_B$ becomes of the order of unity[26,27], a condition in which the strain rate is large enough to generate a significant tension in the network before it spontaneously unbind because of the finite lifetime. In bead based experiments, where $\dot{\gamma}$ is not homogeneous in the system, the natural dimensionless parameter to gauge the onset of non-Newtonian behavior is the ratio $B = v\tau_B/R$ [28] which is the Deborah number of our experiments. In this study, the values of B spans four orders of magnitude, as a combination of the limited range of experimentally accessible velocities and of the large variation in τ_B obtained upon changing T.

Power law fluid behavior is generally believed to emerge as a feature of the transition from Newtonian to non-Newtonian viscosity as a function of the shear rate. To explore this notion in the context of our measurements, we adopted the plainest among the model describing such a transition, namely the Cross model with exponent equal to 1 [29,27],

$$\eta_A = \frac{\eta_0 - \eta_\infty}{1+B} + \eta_\infty \qquad (1)$$

where η_0 and η_∞ are respectively the viscosity in the limit of zero and infinite speed. Eq. 1 accounts for a cross-over from a regime of small structural deformations (i.e. small τ_B, high T, small v) in which the fluid is Newtonian, to a regime of large structural deformations (i.e. large τ_B, low T, large v) in which $\eta_A \propto 1/B \propto v^{-1}$, as in the strong non-Newtonian limit we observe. A simple inspection of Eq. 1 indicates that the smooth transition between these regimes could be thought of as a family of power-law fluids, each verified in a limited range of B, and whose exponent varies with B as $n \approx (1+B)^{-1}$.

The $\eta_A(v)$ dependence expressed in Eq. 1 can be used to fit the measured x(t) (Fig. 3a) by integrating the equation of motion with η_∞ set to the viscosity of water and with η_0 and τ as fitting parameters [see ESI]. The good quality of the fits (lines in Fig. 3a) indicates that all η_A data can be expressed in terms of the two dimensionless quantities $(\eta_A - \eta_\infty)/(\eta_0 - \eta_\infty)$ and B, readily computed from η_0(T) and τ(T) determined for each optical shooting. Indeed, when $\eta_A(v)$ datasets (Fig. 3b) are rescaled using the two dimensionless quantities, they collapse on a universal curve, as shown in Fig. 3d. This collapse supports the notion that the whole behavior of this system reflects a single basic microscopic mechanism with the power-law behavior emerging as a cross-over condition. Such mechanism is also revealed by inspecting the T dependence of the best fit values of η_0 and τ. In Fig. 3e we show η_0 (red triangles, right-hand axis) and τ (blue diamonds, left-hand axis) vs. 1/T. In the same figure we also plot τ_{DLS} (green squares, left-hand axis), the lifetime of thermally induced concentration fluctuations, that we previously measured by Dynamic Light Scattering (DLS) on the same sample [12,17,30] [See ESI].

Despite a significant level of noise, data in Fig. 3e unambiguously indicate that the whole thermal and viscous behavior of the DNA transient network is controlled by a single Arrhenius process. The associated activation enthalpy ΔH can be derived from the slope of the data (dashed line). We find $\Delta H \approx 87$ kcal/mol, compatible with the enthalpy necessary to disrupt the bonds between NS [12,17,30]. Both T dependence and values of the viscous characteristic time τ in Fig. 3e are compatible with the expected inter-NS bond lifetime τ_B, as determined from hybridization kinetic studies[31]. Thus, our observations indicate that $\tau \approx \tau_B$, i.e. the viscous characteristic time matches the characteristic time of the microscopic bonds. Moreover η_0, the zero-velocity limit of the viscosity, is also found to grow according to an equal activation scaling. This is in line with observations in network-forming molecular glasses such as silica [32], and it is generally expected since the characteristic scale of energy in this system is set by the inter-NS bond enthalpy.

Three regimes

The collapse of the data into a single universal curve depending on B indicates that the whole behavior is controlled by the interplay between the shear stress, imposed by the motion of the bead, and the relaxation time of the networks structure. Accordingly, we interpret here our observations as resulting from the evolution through three regimes: the "cluster regime" (Newtonian), the "stretched elastic network" regime (Newtonian) and the "network fracturing" regime (non-Newtonian), pictorially described in Fig. 4.

At high T the bond lifetime is short, and the system is in the cluster regime (Figs. 4a1 and 4a2): NS are either independent or aggregated in small clusters. In this regime, the viscosity is close to that of water (η_w, dotted line in Figs. 3b and 3c), incremented by a correction proportional to the volume fraction of the

suspended particles [33]. Since low valence colloids aggregate into low-density ("empty") structures [34], upon aggregating from single NS into small clusters the effective volume fraction filled by DNA mildly grows while remaining Newtonian.

As T lowers, clusters become large enough to be significantly deformed by the local shear rate produced by the motion of the particle (Fig. 4b1 and 4b2). Because of such deformation, the network locally develops a shear elastic force opposing the bead motion. However, in this regime, the bond lifetime is short enough that the bead does not actively disrupt them, since they spontaneously open fast enough not to ever reach their tearing point.

At low T, instead, the network is percolating and long-lived. In this condition, the bead can proceed only by breaking the bonds (Fig. 4c1 and 4c2) and the work spent to move the bead must equal the energy required to open the inter-NS bonds constraining the motion. Thus, in this regime, the friction force experienced by the bead depends on the number of broken bonds but not on the velocity of the bead, a condition that correspond to the strong shear-thinning behavior experimentally observed at low T.

Quantitative analysis: tearing force

The force and energy required to tear a molecular network are described by the classic Lake-Thomas model and its developments[14,16,35–37]. According to this approach, we can calculate T_0, the ratio of the fracturing energy (E_{FR}) and the cross section of the fracture (A), from structural and energetic parameters of the network:

$$T_0 = \frac{E_{FR}}{A} = \left(\frac{3}{8}\right)^{1/2} \nu L N \mathrm{E_R} \qquad (2)$$

where E_R is the rupturing energy of the single monomer, while ν, L and N are respectively the number density of "active chains" (chains participating in the actual connectivity of the network, excluding dangling chains), the length and the polymerization degree of the ruptured chains.

E_R is in our case very well known since it corresponds to the free energy ΔG(T) involved in the hybridization of the overhangs of the NS. ΔG(T) can be evaluated for our specific DNA sequence by using the standard Nearest-Neighbor model for DNA thermodynamics [13] and is shown in Fig. 3f as a continuous red line.

The number ν of the active chains involved in the tearing process while the bead moves in the DNA NS network can be estimated from the number of nodes in the network which depends on the quantity p(T), the fraction NS arm tips that are bound at a given T. Thanks to our design of the gel, p(T) depends on the thermodynamic parameters involved in the hybridization of the NS sticky end (CGATCG) and can be computed using tools such as NUPAC [38] . p(T), shown in Fig. S3 [see ESI], changes form p = 1 at low T, to p = 0 at about T ≈ 45°. The effect of the change in p is pictorially represented in Figs. 1b and 1c for two representative temperatures 35 °C (p=0.17) and 20 °C (p=0.66). Based on the knowledge of p, we can compute the number density n_3(T) of "active nodes" in the network, i.e. of NS that participate as nodes in the connectivity of large clusters. When p=1, $n_3 = n_{NS}$. For lower p, we need to exclude from n_3(T) all NS having less than three connected bonds and all NS connected to dangling branches. n_3(T) can be calculated from p(T) either adopting the theory for tree-like structures[15,37] or can be numerically computed using a recursive procedure on a 3d model of the network [see ESI]. The two procedures are limited to conditions where p is large enough (p>0.5) and give comparable results [Fig. S5].

Finally, because of the valence f=3 of the active NS:

$$\nu(T) = \frac{3}{2} n_3(T) \qquad (3)$$

When p=1, $L = \ell_0$, the distance between two NS centers (14.5 nm, see ESI) and N, the polymerization length, is 1. As T grows, we can estimate *L* by scaling it with the mean distance between active nodes, $L \sim \ell_0 (n_{NS}/n_3)^{-\frac{1}{3}}$, while $N = L/\ell_0$. Thus, the product $L \cdot N$ becomes:

$$L \cdot N \sim \ell_0 (n_3/n_{NS})^{\frac{2}{3}} \qquad (4).$$

As the bead move forward of a length Δx through the network, the minimum area over which the bonds need to be ruptured is approximately $2R\Delta x$. From Eq. 2:

$$T_0 = \frac{E_{FR}}{2R\Delta x} = \frac{F_{FR}}{2R} \qquad (5)$$

In Eq. 5 we introduce the tearing force F_{FR}, which should be compare to the force measured to propel the bead in the network fracturing regime. Combining equations (5),(4),(2) and using the calculated ΔG(T) and $\nu(T)$ we obtain for T = 22°C (the lowest considered in this study), F_{FR}= 85 pN. This value is in good agreement with the observation, as it can be recognized in Fig. 3c, where have marked $F_{FR}(T)$ with a dashed line. An alternate evaluation of $F_{FR}(T)$, yielding a similar result (≈ 75 pN) can be obtained from R, ΔG(T) and n_3(T) via simple geometrical and physical assumptions [see ESI].

Quantitative analysis: Newtonian to non-Newtonian crossover

We now turn to discussing the crossover between the stretched elastic network regime and the network fracturing regime, its nature, the T at which it is found and its width. The quantitative agreement between measured and computed F_{FR} at low T suggests that the transition to non-Newtonian fluid is produced by an increasing relevance of the bond breaking mechanism. In the stretched elastic network regime, introduced in the first paragraph of this section, the amplitude of the elastic force is limited by the bond lifetime that sets a maximum value for the local shear $\gamma_M = \dot{\gamma}\tau_B$ since in this regime bonds are not actively ruptured, but rather spontaneously open because of their limited lifetime. This limit corresponds to an elastic tangential stress $\sigma_E = G'^{\dot{\gamma}}\tau_B$, where G' is the shear elastic modulus of the network. The spontaneous opening of the bonds dissipates the elastic energy accumulated by the deformation so that σ_E contributes to the effective Newtonian viscosity, the total stress becoming $\sigma = (\eta_w + G'\tau_B)\dot{\gamma}$ and the force on the bead $F = 6\pi R(\eta_w + G'\tau_B)v$, where η_w is the viscosity of water.

This regime extends at low T until the elastic energy E_{el} stored in each bond becomes comparable with ΔG(T), a condition that

determines the crossover temperature between Newtonian and non-Newtonian behavior. E_{el} can be estiamated from G', τ_B, R, v, and n_3 [see ESI]. G'(T) can be evaluated by the standard phantom network model [39] as $G' = k_B T 3/2\, n_3 (1 - 2/f)$, where in our case f = 3. τ_B is available from our data (Fig. 3e). The resulting $E_{el}(T)$ is shown in Fig. 3f for three values of v (60 μm/s dotted blue line, 10 μm/s continuous blue line, 3 μm/s blue dashed line). As visible, upon lowering T, E_{el} becomes larger than ΔG (red line), which indicates that the network is stressed beyond its tearing threshold. The crossing between the computed values of $E_{el}(T)$ and $\Delta G(T)$, gives an estimate for the T where we expect the crossover between the stretched elastic network regime and the network fracturing regime to take place. We find such T to be approximately around 28°C, an estimate that agrees with the T at which the power-law exponent is found to markedly change (purple shading).

A more refined quantitative analysis of the crossover toward non-Newtonian viscosity can be formulated on the basis of the "soft glass rheology" model in Ref. 2, which describes the viscoelasticity of soft materials whose structure is stabilized by bonds that require an activation energy to be broken. When mechanically perturbed, the system may thus be found in metastable states, depending on the time-scale of the action. According to this model, the transition from Newtonian and non-Newtonian indeed occurs through power-law fluid behavior. The transition takes place when the difference $\Delta G - E_{el}$ lays in a given range of thermal noise, namely when $2\ k_BT > \Delta G - E_{el} > 1\ k_BT$. In this range, the system shows a power-law fluid behavior whose exponent ranges from n ≈ 0.2 to n ≈ 0.8, respectively. Because of the strong T dependence of the energies involved in the DNA NS bonds, this energy range is found in our system by changing T of a few degrees only. This can be appreciated in the construction of Fig. 3f, in which we have marked by orange shading the energy range (ΔG - 2 k_BT, ΔG - 1 k_BT) [see. ESI], by grey shading the T range in which such energy interval is crossed by the elastic energy for v = 10 μm/s (continuous blue line) and by black squares the expected values of *n* (n = 0.2 and n = 0.8) at the two boundaries of the interval. Fig. 3f enables comparing the outcome from this theoretical estimate (black squares and grey shaded area) and the experimental results (color dots and purple-shaded area). Remarkably, the quantitative prediction of the model, in which we used only literature information and geometrical data, well approximates the observations both in the crossover temperature – expected to be only a few degrees above the observations – and in the width the crossover – of the order of 3 degrees.

Conclusions

The model DNA network investigated here by active microrheology enables to successfully explore the complex viscous behavior of network forming systems. We find that in a narrow T range the NS system crosses over from Newtonian fluidity to strong shear thinning viscosity through power-law fluid states of decreasing exponent.

All the key features we experimentally observe can be quantitatively understood thanks to a detailed knowledge of the microscopic structure of the gel. Specifically, we could explain:

- the existence of a regime at low T in which the friction is independent on velocity, $\eta_A \propto v^{-1}$, and the value of the force (F_{FR} ≈ 85 pN) required to set the particle in motion at T = 22 °C;
- the temperature at which the Newtonian to non-Newtonian crossover occurs, which we determine to be T ≈ 28°C, only 2 °C above the observed one;
- the existence of a smooth transition between Newtonian and strong non-Newtonian behavior thorough power-law fluids whose exponents smoothly depend on T in a T range of 2-3 °C width, as experimentally found. This prediction relies on the "soft glass rheology" model of Ref. 2.

This study indicates that the whole set of mechanical properties of transient networks can be reduced to two key ingredients: the energy scale of the single bond and the network topology. All the quantitative predictions listed above ultimately depend on these two parameters solely. Thus, by exploiting this knowledge, we could design DNA hydrogels having topology, density of bonds, and bond strength such to tailor the viscous properties of the resulting material: the frictional force, and the location and sharpness of the Newtonian to non-Newtonian transition.

Finally, it is worth noticing that the DNA NS hydrogel, which we previously proposed as a model of strong glass formers for its equilibrium and thermodynamic properties [17], shares with silica – the archetype of glass forming liquids – also important rheological properties, such as the proportionality between viscosity and relaxation time (as in our Fig. 3e) and the collapse of η(v) once properly rescaled (as in our Fig. 3d) [32].

Conflicts of interest

There are no conflicts to declare

Acknowledgements

We thank P. Malgaretti and G. Zanchetta for the fruitful discussion.

References

1 D. T. N. Chen, Q. Wen, P. A. Janmey, J. C. Crocker and A. G. Yodh, *Annu. Rev. Condens. Matter Phys.*, 2010, **1**, 301–322.

2 P. Sollich, *Phys. Rev. E*, 1998, **58**, 738–759.

3 M. Guvendiren, H. D. Lu and J. A. Burdick, *Soft Matter*, 2012, **8**, 260–272.

4 K. Holmberg, B. Jönsson, B. Kronberg and B. Lindman, *Surfactants and Polymers in Aqueous Solution*, John Wiley & Sons, Ltd, Chichester, UK, 2002.

5 R. D. Jenkins, C. A. Silebi and M. S. Elaasser, *Acs Symp. Ser.*, 1991, **462**, 222–233.

6 T. Annable, R. Buscall, R. Ettelaie and D. Whittlestone, *J. Rheol. (N. Y. N. Y).*, 1993, **37**, 695–726.

7 I. Kunita, K. Sato, Y. Tanaka, Y. Takikawa, H. Orihara and T. Nakagaki, *Phys. Rev. Lett.*, 2012, **109**, 248303.

8 R. E. Buxbaum, T. Dennerll, S. Weiss and S. R. Heidemann, *Science*, 1987, **235**, 1511–4.

9 B. Huber, M. Harasim, B. Wunderlich, M. Kröger and A. R. Bausch, *ACS Macro Lett.*, 2014, **3**, 136–140.

10 B. J. Gold, C. H. Hövelmann, N. Lühmann, W. Pyckhout-Hintzen, A. Wischnewski and D. Richter, *J. Rheol. (N. Y. N. Y).*, 2017, **61**, 1211–1226.

11 D. Xu and S. L. Craig, *Macromolecules*, 2011, **44**, 7478–7488.

12 S. Biffi, R. Cerbino, F. Bomboi, E. M. Paraboschi, R. Asselta, F. Sciortino and T. Bellini, *Proc. Natl. Acad. Sci. U. S. A.*, 2013, **110**, 15633–7.

13 J. SantaLucia and D. Hicks, *Annu. Rev. Biophys. Biomol. Struct.*, 2004, **33**, 415–40.

14 G. J. Lake and A. G. Thomas, *Proc. R. Soc. A Math. Phys. Eng. Sci.*, 1967, **300**, 108–119.

15 D. R. Miller and C. W. Macosko, *Macromolecules*, 1976, **9**, 206–211.

16 Y. Akagi, J. P. Gong, U. Il Chung and T. Sakai, *Macromolecules*, 2013, **46**, 1035–1040.

17 S. Biffi, R. Cerbino, G. Nava, F. Bomboi, F. Sciortino and T. Bellini, *Soft Matter*, 2015, **11**, 3132–3138.

18 P. Minzioni, R. Osellame, C. Sada, S. Zhao, F. G. Omenetto, K. B. Gylfason, T. Haraldsson, Y. Zhang, A. Ozcan, A. Wax, F. Mugele, H. Schmidt, G. Testa, R. Bernini, J. Guck, C. Liberale, K. Berg-Sørensen, J. Chen, M. Pollnau, S. Xiong, A.-Q. Liu, C.-C. Shiue, S.-K. Fan, D. Erickson and D. Sinton, *J. Opt.*, 2017, **19**, 93003.

19 T. Yang, Y. Chen and P. Minzioni, *J. Micromechanics Microengineering*, 2017, **27**, 123001.

20 T. Yang, G. Nava, V. Vitali, F. Bragheri, R. Osellame, T. Bellini, I. Cristiani and P. Minzioni, *Micromachines*, 2017, **8**, 65.

21 N. Bellini, F. Bragheri, I. Cristiani, J. Guck, R. Osellame and G. Whyte, *Biomed. Opt. Express*, 2012, **3**, 2658–68.

22 L. Ferrara, E. Baldini, P. Minzioni, F. Bragheri, C. Liberale, E. Di Fabrizio and I. Cristiani, *J. Opt.*, 2011, **13**, 75712.

23 R. P. Chhabra and J. F. Richardson, *Elsevier*, 2008, 518.

24 W. B. Russel, D. A. Saville and W. R. Schowalter, *Colloidal dispersions*, Cambridge University Press, 1989.

25 M. J. Whitney and G. J. Rodin, *Int. J. Non. Linear. Mech.*, 2001, **36**, 947–953.

26 R. G. Larson, *The Structure and Rheology of Complex Fluids.*, Oxford University Press, 1999.

27 M. M. Cross, *Rheol. Acta*, 1979, **18**, 609–614.

28 A. Ziegenhagen, *Appl. Sci. Res.*, 1964, **14**, 43–56.

29 M. M. Cross, *J. Appl. Polym. Sci.*, 1969, **13**, 765–774.

30 G. Nava, M. Rossi, S. Biffi, F. Sciortino and T. Bellini, *Phys. Rev. Lett.*, 2017, **119**, 78002.

31 N. F. Dupuis, E. D. Holmstrom and D. J. Nesbitt, *Biophys. J.*, 2013, **105**, 756–66.

32 I. Farnan and J. F. Stebbins, *Science (80-.).*, 1994, **265**, 1206–1209.

33 E. Guyon, J.-P. Hulin, L. Petit and C. D. Mitescu, *Physical Hydrodynamics, 2nd Edn*, Oxford University Press, 2015.

34 E. Bianchi, J. Largo, P. Tartaglia, E. Zaccarelli and F. Sciortino, *Phys. Rev. Lett.*, 2006, **97**, 1–4.

35 F. Lange, K. Schwenke, M. Kurakazu, Y. Akagi, U. Il Chung, M. Lang, J. U. Sommer, T. Sakai and K. Saalw??chter, *Macromolecules*, 2011, **44**, 9666–9674.

36 Y. Akagi, T. Katashima, Y. Katsumoto, K. Fujii, T. Matsunaga, U. Il Chung, M. Shibayama and T. Sakai, *Macromolecules*, 2011, **44**, 5817–5821.

37 Y. Akagi, H. Sakurai, J. P. Gong, U. Chung and T. Sakai, 2015, **144905**, 1–7.

38 J. N. Zadeh, C. D. Steenberg, J. S. Bois, B. R. Wolfe, M. B. Pierce, A. R. Khan, R. M. Dirks and N. A. Pierce, *J Comput Chem*, 2011, **32**, 170–173.

39 M. Rubinstein and R. Colby, *Polymer physics*, Oxford University Press, 2003.

FIGURE CAPTIONS

1 Description of the transient network based on interacting DNA nanostars (NS). **a**: Each DNA nanoparticle is shaped as a three-armed star. Each arm terminates with a sticky spot that provides NS with mutual attraction, thus making them valence 3 (f=3) particles. The sticky terminals consist in 6 base-long self-complementary overhanging sequences, which at low T hybridize with the overhangs of other NS. **b**,**c**: Pictorial sketches describing the T dependence of the NS aggregation state. **b**: at T = 35 °C, the fraction of bound terminals is p = 0.17, and the NS are dispersed as monomers or small clusters. **c**: at T = 20 °C, the

fraction of bound terminals is p = 0.66, and the NS are bound into a percolating network.

2 Microfluidic-based active microrheology. a,**b**: the optofluidic chip (**a**) comprizes a straight fluidic channel having section 150 μm x 150 μm and two waveguide carrying counter-propagating beams perpendicularly to the channel as described in the sketch (**b**). Micro-beads are trapped and put in motion by modulating the light power carried by the two waveguides. **c**: the experiment is prepared by unbalancing the beams and trapping the bead near a channel wall. In the sketch, the light power coming from the right-hand side (marked as LASER ON*) is larger than the opposite one. **d**: as the stronger beam is shuttered, the bead is shot across the channel. **e**: example of position (x) dependence of the optical force for a given laser power. **f**: excerpt of a typical time-lapse sequence of a shooting procedure. **g**: by tracking the bead on the recorded video, its motion *x(t)* (black line) could be determined with 1μm resolution.

3 **Viscous behavior of the DNA network**. Viscosity measurements were performed in a range of temperatures T represented by a color code adopted throughout the figure. **a**: bead motion x(t) measured for a choice of T and light powers (empty dots) and their fitting with Eq. 1 (lines). **b**: for each optical shooting, the bead speed v(x) was determined from x(t) and used to extract the apparent viscosity η_A as a function of v (colored squares). Dotted line: water viscosity. Dashed line: η_A in the network fracturing regime at T = 22°C. **c**: from the same data, we determined the force F vs. v. Dotted line: F in pure water. Dashed line: F in the network fracturing regime at T = 22°C. **d**: data in panel **b** are rescaled using two dimensionless quantities based on $\eta_0(T)$ and $\tau(T)$. The scaling of $\eta_A(T)$ leads to the collapse of all measured data. **e**: the fitting of x(t) (panel **a**) enabled determining the values of $\tau(T)$ (blue diamonds, left-hand axis) and $\eta_0(T)$ (red triangles, right-hand axis) for each optical shooting. $\tau_{DLS}(T)$ determined via Dynamic Light Scattering [see ESI] are also shown (green squares, left-hand axis). **f**: T dependence of the exponents *n* of the power law fluid (colored dots, right-hand axis). The experimental crossover range (from n=0.8 to n=0.2) is marked by purple shading. Elastic energy per bond E_{el} caused by the deformation caused by the bead moving at a speed v (blue lines, left-hand axis; dotted line, v=3 μm/s; continuous line, v=10 μm/s; dashed line, v=60 μm/s). Free energy per NS-NS bond ΔG (red line, left-hand axis). The crossover from n=0.8 to n=0.2 predicted by the model in Ref. 2 is obtained by the crossing of E_{el} with ΔG-k_BT and ΔG-$2k_BT$ (orange lines). The construct in the figure, built with E_{el} at v=10 μm/s, predicts the crossover to take place in the grey shaded region. The black squares represent the predicted conditions of n=0.2 and n=0.8.

4 Three regimes in the transition between Newtonian to non-Newtonian fluid. Upon lowering the temperature, the system evolves through three states, here pictorially described at the bead length scale (panels **1**, at the left-hand side) and at the NS length scale (panels **2**, at the right-hand side). In the drawing the NS density is marked by purple shading. In the Newtonian "cluster regime" the system is a dispersion of independent NS or small clusters of NS (**a1**, **a2**). In the Newtonian "stretched elastic network" regime the NS network is extended but the bond lifetime is short enough that the bead motion stresses the network but does not break the bonds (**b1**, **b2**). In the non-Newtonian "network fracturing" regime the network is long lived and the bead moves by breaking the bonds to produce an opening through the network (**c1**, **c2**).

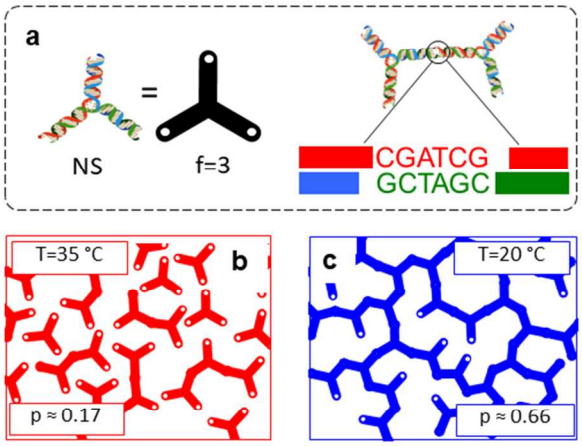

Fig. 1: Description of the transient network based on interacting DNA nanostars (NS). a: Each DNA nanoparticle is shaped as a three-armed star. Each arm terminates with a sticky spot that provides NS with mutual attraction, thus making them valence 3 (f=3) particles. The sticky terminals consist in 6 base-long self-complementary overhanging sequences, which at low T hybridize with the overhangs of other NS. b,c: Pictorial sketches describing the T dependence of the NS aggregation state. b: at T = 35 °C, the fraction of bound terminals is p = 0.17, and the NS are dispersed as monomers or small clusters. c: at T = 20 °C, the fraction of bound terminals is p = 0.66, and the NS are bound into a percolating network.

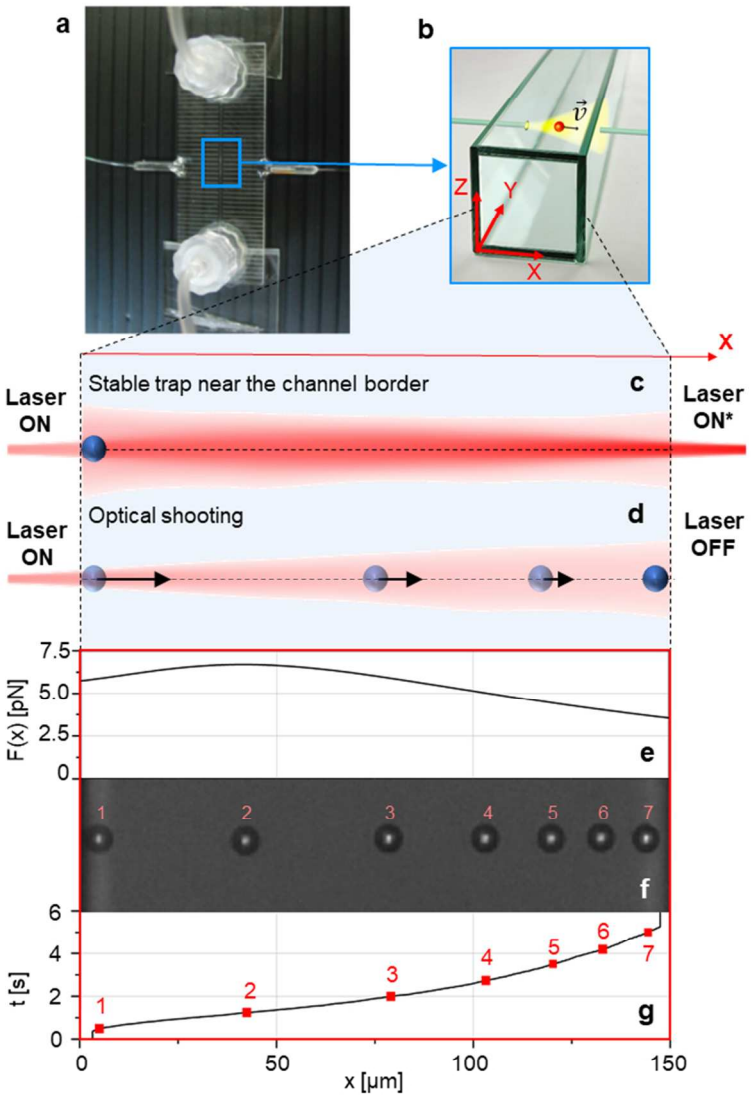

Fig. 2: Microfluidic-based active microrheology. a,b: the optofluidic chip (a) comprizes a straight fluidic channel having section 150 μm x 150 μm and two waveguide carrying counter-propagating beams perpendicularly to the channel as described in the sketch (b). Micro-beads are trapped and put in motion by modulating the light power carried by the two waveguides. c: the experiment is prepared by unbalancing the beams and trapping the bead near a channel wall. In the sketch, the light power coming from the right-hand side (marked as LASER ON*) is larger than the opposite one. d: as the stronger beam is shuttered, the bead is shot across the channel. e: example of position (x) dependence of the optical force for a given laser power. f: excerpt of a typical time-lapse sequence of a shooting procedure. g: by tracking the bead on the recorded video, its motion x(t) (black line) could be determined with 1μm resolution.

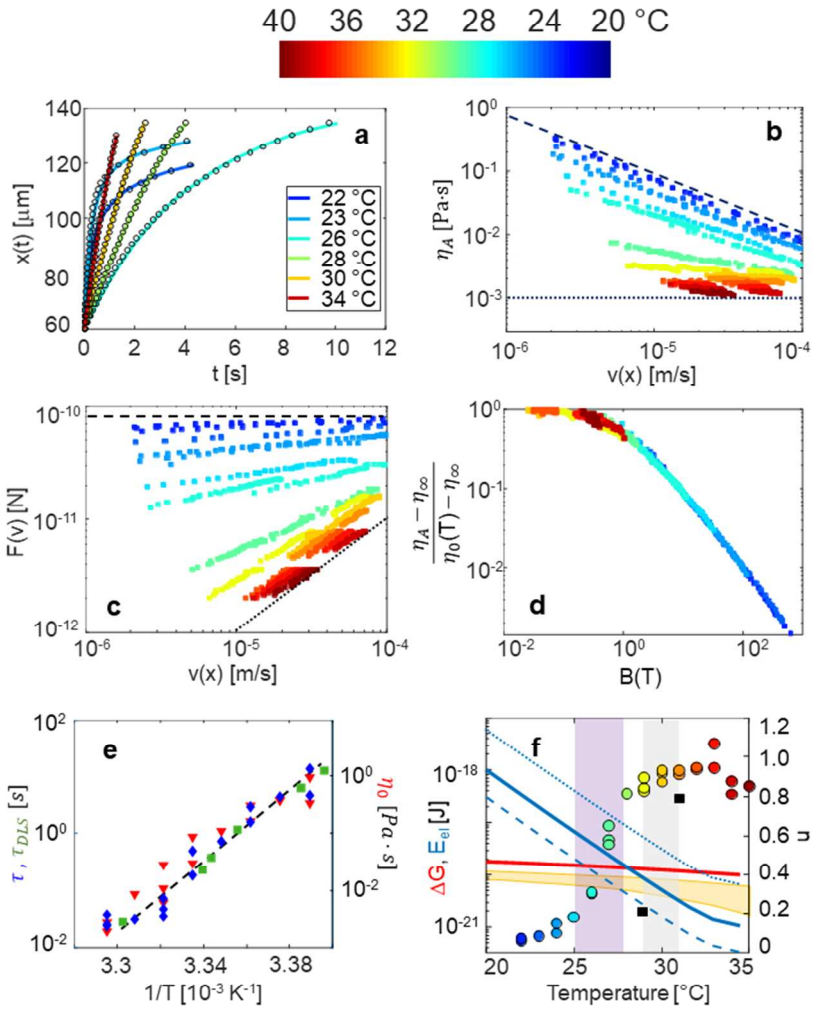

Fig. 3: Viscous behavior of the DNA network. Viscosity measurements were performed in a range of temperatures T represented by a color code adopted throughout the figure. a: bead motion x(t) measured for a choice of T and light powers (empty dots) and their fitting with Eq. 1 (lines). b: for each optical shooting, the bead speed v(x) was determined from x(t) and used to extract the apparent viscosity ηA as a function of v (colored squares). Dotted line: water viscosity. Dashed line: ηA in the network fracturing regime at T = 22°C. c: from the same data, we determined the force F vs. v. Dotted line: F in pure water. Dashed line: F in the network fracturing regime at T = 22°C. d: data in panel b are rescaled using two dimensionless quantities based on η0(T) and τ(T). The scaling of ηA(T) leads to the collapse of all measured data. e: the fitting of x(t) (panel a) enabled determining the values of τ(T) (blue diamonds, left-hand axis) and η0(T) (red triangles, right-hand axis) for each optical shooting. τDLS(T) determined via Dynamic Light Scattering [see S.I.] are also shown (green squares, left-hand axis). f: T dependence of the exponents n of the power law fluid (colored dots, right-hand axis). The experimental crossover range (from n=0.8 to n=0.2) is marked by purple shading. Elastic energy per bond Eel caused by the deformation caused by the

bead moving at a speed v (blue lines, left-hand axis; dotted line, v=3 μm/s; continuous line, v=10 μm/s; dashed line, v=60 μm/s). Free energy per NS-NS bond ΔG (red line, left-hand axis). The crossover from n=0.8 to n=0.2 predicted by the model in Ref. 2 is obtained by the crossing of Eel with ΔG-kBT and ΔG-2kBT (orange lines). The construct in the figure, built with Eel at v=10 μm/s, predicts the crossover to take place in the grey shaded region. The black squares represent the predicted conditions of n=0.2 and n=0.8.

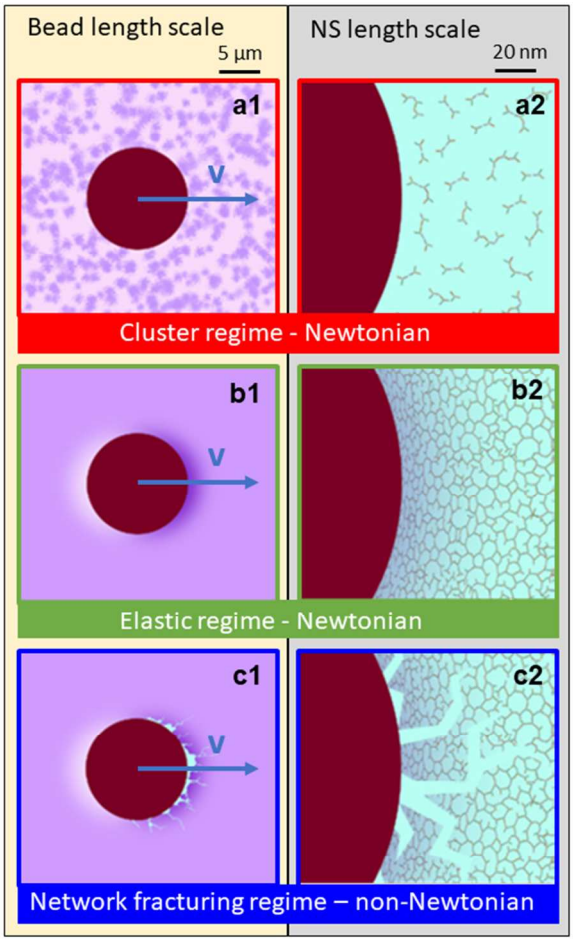

Fig. 4: Three regimes in the transition between Newtonian to non-Newtonian fluid. Upon lowering the temperature, the system evolves through three states, here pictorially described at the bead length scale (panels 1, at the left-hand side) and at the NS length scale (panels 2, at the right-hand side). In the drawing the NS density is marked by purple shading. In the Newtonian "cluster regime" the system is a dispersion of independent NS or small clusters of NS (a1, a2). In the Newtonian "stretched elastic network" regime the NS network is extended but the bond lifetime is short enough that the bead motion stresses the network but does not break the bonds (b1, b2). In the non-Newtonian "network fracturing" regime the network is long lived and the bead moves by breaking the bonds to produce an opening through the network (c1, c2).